Dalton Transactions

ROYAL SOCIETY OF CHEMISTRY

PAPER

View Article Online
View Journal | View Issue





Cite this: *Dalton Trans.*, 2020, **49**, 17243

# Dinuclear uranium(VI) salen coordination compound: an efficient visible-light-active catalyst for selective reduction of $CO_2$ to methanol†

Mohammad Azam, *[a] Umesh Kumar, *[b] Joshua O. Olowoyo,[b] Saud I. Al-Resayes,[a] Agata Trzesowska-Kruszynska,[c] Rafal Kruszynski,[c] Mohammad Shahidul Islam,[a] Mohammad Rizwan Khan,[a] S. F. Adil,[a] Mohammad Rafique Siddiqui,[a] Fahad Ahmed Al-Harthi,[a] Abdul Karim Alinzi,[a] Saikh Mohammad Wabaidur,[a] Masoom Raza Siddiqui,[a] Mohammed Rafi Shaik,[a] Suman L. Jain,[b] M. Amin Farkhondehfal[d] and Simelys Hernàndez[e]

A new dinuclear uranyl salen coordination compound, $[(UO_2)_2(L)_2]\cdot 2MeCN$ [L = 6,6′-((1*E*,1′*E*)-((2,2-dimethylpropane-1,3-diyl)bis(azaneylylidene))-bis(methaneylylidene))bis(2-methoxyphenol)], was synthesized using a multifunctional salen ligand to harvest visible light for the selective photocatalytic reduction of $CO_2$ to MeOH. The assembling of the two U centers into one coordination moiety *via* a chelating–bridging doubly deprotonated tetradentate ligand allowed the formation of U centers with distorted pentagonal bipyramid geometry. Such construction of compounds leads to excellent activity for the photocatalytic reduction of $CO_2$, permitting a production rate of 1.29 mmol $g^{-1}$ $h^{-1}$ of MeOH with an apparent quantum yield of 18%. Triethanolamine (TEOA) was used as a sacrificial electron donor to carry out the photocatalytic reduction of $CO_2$. The selective methanol formation was purely a photocatalytic phenomenon and confirmed using isotopically labeled $^{13}CO_2$ and product analysis by $^{13}C$-NMR spectroscopy. The spectroscopic studies also confirmed the interaction of $CO_2$ with the molecule of the title complex. The results of these efforts made it possible to understand the reaction mechanism using ESI–mass spectrometry.

Received 24th July 2020,
Accepted 25th October 2020

DOI: 10.1039/d0dt02620d

rsc.li/dalton

## Introduction

The depletion of fossil fuel reserves and the continuous increase in the $CO_2$ concentration in the atmosphere have led to various environment-related issues.[1,2] Therefore, the photocatalytic reduction of $CO_2$ could be a sustainable technology for reducing $CO_2$ emissions and producing useful chemicals and fuels, subsequently providing environmental remediation to global warming and the future depletion of fossil energy resources.[3,4] Various semiconductor photocatalysts, such as oxide-based semiconductors, have been used for the conversion of $CO_2$ into useful compounds.[5–9] However, the poor visible light absorbance, low conversion degree, and high charge recombination have limited the usage of these systems.[8,9]However, after tuning the properties of the catalytic system with correct molecular structure, molecular catalysts such as dinuclear rhenium–bipyridine molecular assemblies,[10,11] cobalt–porphyrin compounds,[12] mononuclear iridium hetero-ligand-based molecules (*e.g.*, terpyridine/2-phenylpyridine),[13] iron(0)–porphyrin compounds,[14] cobalt–aminopyridine compounds,[15] and manganese and iron-based coordination polymers with pyridyl-salen ligand can be effective in the photocatalytic reduction of $CO_2$, especially in CO generation.[16] Similarly, the trinuclear ruthenium polyazine-GO-phen compound,[17] ruthenium trisphenanthroline assemblies,[18] and Mn(I) hydridocarbonyl PNP pincer-type complexes have been developed as photocatalysts for the conversion of $CO_2$ to MeOH.[19]

Uranium-containing compounds have been used extensively in various catalytic reactions, *i.e.* the alcoholysis of

[a]*Department of Chemistry, College of Science, King Saud University, P. O. Box 2455, Riyadh 11451, Kingdom of Saudi Arabia. E-mail: azam_res@yahoo.com, mhashim@ksu.edu.sa; Tel: +966-1-4675982*
[b]*Chemical Science Division, CSIR-Indian Institute of Petroleum Dehradun, India-248005. E-mail: umesh_kumar@iip.res.in*
[c]*Institute of General and Ecological Chemistry, Lodz University of Technology, Zeromskiego 116, 90-924 Lodz, Poland*
[d]*Center for Sustainable Future Technologies @POLITO, Instituto Italiano di Tecnologia, Via Livorno 60, 10144 Turin, Italy*
[e]*Department of Applied Science and Technology, Politecnico di Torino, C.so Ducadegli Abruzzi 24, 10129 Turin, Italy*

†Electronic supplementary information (ESI) available. CCDC 1567193. For ESI and crystallographic data in CIF or other electronic format see DOI: 10.1039/d0dt02620d

esters, the Michael addition, Diels–Alder reactions and polymerizations,[20] photochemical reduction,[21] thermocatalysis,[22] photocatalysis,[23] and axial uranium–oxygen bond activation.[24] The uranyl ion (dioxouranium(VI) ion, $UO_2^{2+}$), a highly stable and dominant functional species, plays a key role in the coordination chemistry of uranium.[25]

Furthermore, the uranyl ion absorbs visible radiation, and produces a strong emission of photons for specific excitation wavelengths. The high photocatalytic reactivity of uranyl-containing coordination compounds is attributed to their high quantum efficiency up to 1 with efficient electron transfer between the photoexcited $*UO_2^{2+}$ and organic molecules.[26,27] The rich and diverse photochemistry, together with the high oxidation potential, makes the uranyl ion a promising candidate in the synthesis of new photocatalysts.[28–31] To the best of our knowledge, uranyl(VI) salen coordination compounds have never been explored as photocatalysts for the reduction of $CO_2$. These factors led us to develop a new dinuclear uranyl coordination compound possessing a salen ligand and, subsequently, to the first-ever exploration of its role in the photocatalytic reduction of $CO_2$ under visible light irradiation.

# Experimental

### Materials and methods

TEOA was purchased from Merck, HPLC grade MeCN from SD Fine-Chem Limited, $CO_2$ and methane ($CH_4$) (99.9995%) from Sigma Gases, India. HPLC grade water was used in all experiments. Uranyl acetate was obtained from BDH. All other materials used in the synthesis of the title complex were bought from Sigma Chemical Co. and used as received. The salen ligand was synthesized as described in the literature.[32] The new uranyl complex was characterized at room temperature using $^1H$ and $^{13}C$ NMR spectroscopy with the use of JEOL instrument at 400 MHz and 100 MHz, respectively. The infrared spectrum was recorded with a PerkinElmer 621 spectrometer (spectral range: 400 to 4000 $cm^{-1}$, sample as KBr pellets). Elemental analysis was performed with the usage of an Elementar vario EL elemental analyzer. Electronic spectra were recorded with an Evolution $^{TM}$300 UV-vis spectrometer.

### Synthesis of the uranyl compound

$UO_2(OAc)_2{\cdot}2H_2O$ [0.172 g, $0.405 \times 10^{-3}$ mol] was added to 20 mL of EtOH solution of the ligand [0.150 g, $0.405 \times 10^{-3}$ mol].[32] The reaction mixture was vigorously stirred until its color turned orange, and the uranyl compound was precipitated out. After continuous stirring for 5 h, the formed precipitate was filtered, washed in turn with diethyl ether and hexane, and dried at room temperature. The freshly prepared compound was recrystallized from MeCN at room temperature, and the orange crystals grew after a few days.

Yield: 68.5%. Empirical formula $C_{46}H_{54}N_6O_{12}U_2$, Elemental analysis: calculated: C, 40.65, H, 4.00; N, 6.18; found C, 40.63, H, 3.95; N, 6.15%; $^1H$ NMR ($CDCl_3$): $\delta$ (ppm) 8.31(s, 4H, –CH═N), 6.79–6.99 (m, 12H, Ar–H), 3.48 (s, 8H, $-CH_2$), 1.05 (s, 12H, –C–$(CH_3)_2$; $^{13}C$ NMR ($CDCl_3$): $\delta$ (ppm) = 165.7(–*C*H═N), 24.2 (–C(*C*$H_3)_2$), 56.0 (–*C*$(CH_3)_2$), 67.3 (–C–(*C*$H_2)_2$), 36.1 (–O*C*$H_3$), 152.0 (Ar–*C*–O–).

### Crystal structure determination

The X-ray intensity data for the orange-colored prism crystal were recorded on a Rigaku Synergy Dualflex automatic diffractometer equipped with Pilatus 300 K detector with mirror monochromated $CuK_\alpha$ ($\lambda$ = 1.54184 Å, micro-focus sealed Photon Jet X-ray tube) radiation at a temperature of 100.0(1) K. The unit cell parameters were obtained from 36 344 strongest reflections. Details concerning crystal data and refinement are given in the ESI Table S1.† Anisotropic parameters were applied to refine all non-hydrogen atoms. The SHELXS,[33] SHELXL[34] and SHELXTL[35] programs were used for all the calculations. Atomic scattering factors were taken from International Tables for Crystallography.[36] Selected bond lengths are listed in the ESI Table S2,† and intermolecular interactions are listed in the ESI Table S3.†

### Physicochemical measurements

The intermediate species formed during the photocatalytic reduction of $CO_2$ were analyzed with an Agilent 6545 Q-TOF mass spectrometer (M/s Agilent Technologies, USA), resolution: 30 000 (FWHM) ionization: electrospray ionization, positive ion mode sample introduction: flow injection (mobile phase MeCN : $H_2O$ 80 : 20 v/v), 0.3 mL $min^{-1}$ sample injection volume: 1 μl, scan range: *m*/*z* 50–1700.

$^1H$- and $^{13}C$-NMR spectra were recorded on a Bruker Avance III – 500 MHz NMR spectrometer. 200 μL of the sample was dissolved in 100 μL of $D_2O$. In $^1H$-NMR analysis, the number of scans and the delay time were 32 and 10 s, respectively, while in $^{13}C$-NMR analysis, these values were 8000 and 5 s, respectively.

### Photocatalytic reduction of $CO_2$

The photocatalytic reduction of carbon dioxide was performed in a closed quartz reactor with gas recirculation and 50 $cm^3$ internal volume. The reactor was equipped with a gas inlet, gas outlet, gas sampling port, and liquid sampling system. 5.0 mg of the photocatalyst was suspended in the 20 mL mixture of MeCN + $H_2O$ (18 : 2 v/v in mL) or MeCN + TEOA + $H_2O$ (16 : 2 : 2 v/v in mL) and ultra-sonicated for 10 min to obtain a homogeneous dispersion. TEOA was used as a sacrificial electron donor for the reduction of $CO_2$. To remove the dissolved gases, the reaction mixture was evacuated and subsequently purged with $N_2$ 10 times. In the next step, the reaction mixture was purged and saturated with $CO_2$ for 30 min, and then pressurized with $CO_2$ at 1.1 bar. The photocatalytic system was illuminated by a 20 W visible light LED lamp (Syska, cold white LED, 20 μW $cm^{-2}$) to drive the reaction. The intensity of incident light intensity inside the photoreactor was measured using a UVP 97-0015-02/UVX digital radiometer. Small aliquots of gas and liquid samples were taken out periodically after every 2 h of irradiation, and analyzed with a gas chromatograph (GC) (PerkinElmer Clarus 680 equipped

 

with FID and TCD detectors, plot-Q and ShinCarbon columns).

A small aliquot of the liquid phase was withdrawn with the help of a long needle, filtered through the membrane filter and 1 μL of it was injected into the GC using an autosampler. The product formed in liquid phase ($CH_3OH$) was analyzed by GC-FID (carrier gas flow rate 20 mL $min^{-1}$, $H_2$: 35 mL $min^{-1}$, air: 350 mL $min^{-1}$, makeup flow: 27 mL $min^{-1}$, injector temperature: 250 °C, and FID detector temperature: 275 °C). The gaseous product was identified by withdrawing 20 μL sample and analyzed with GC-TCD using a ShinCarbon packed column (reference flow: 45 mL $min^{-1}$, argon flow: 2 mL $min^{-1}$), injector temperature: 220 °C, TCD detector temperature: 200 °C.

To ascertain the products obtained from the photocatalytic reduction of $CO_2$, a series of blank experiments were performed in a preconditioned reactor under the following conditions: (a) in the MeCN + $H_2O$ mixture without the photocatalyst; (b) in the MeCN + $H_2O$ + TEOA mixture without the photocatalyst; (c) in the MeCN + $H_2O$ + TEOA mixture, with the photocatalyst and saturated with $N_2$, in the absence of $CO_2$; (d) in the MeCN + $H_2O$ + TEOA mixture, with the photocatalyst and saturated with $CO_2$, kept under dark conditions (absence of light). No carbonaceous product was detected in the above blank tests, which confirmed that the reaction was solely visible light assisted, and the synthesized methanol resulted from the reduction of $CO_2$, and not from the degradation of any other organic molecule present in the reaction mixture. The system containing 0.5 mg of the catalyst was pre-conditioned by repeatedly applying vacuum and purging with $N_2$ to remove the other dissolved gases before purging with $CO_2$ and applying visible light irradiation.

The isotopic $^{13}CO_2$ (99.99% purity, Cambridge Isotope Laboratories) was also used to confirm whether the photocatalytic reduction product formed is solely from the reduction of $CO_2$. The formed $^{13}CH_3OH$ was analyzed by $^{13}C$ NMR. The quantum yield for the production of methanol was calculated by the equation given below:

$$\Phi_{MEOH},\ \% = \frac{6 \times \text{moles of product} \times \text{electrons required for reduction}}{\text{moles of the incident photon}} \times 100.$$

### Electrochemical studies

The electrochemical tests were carried out with a Rotating Ring Disk Electrode Apparatus (RRDE-3A from Biologic). The prepared ink contained 5 mg of the catalyst added to 45 microliters of Nafion 117 5% solution in a mixture of lower aliphatic alcohols, $H_2O$ and 1.5 mL of $C_2H_5OH$. The prepared ink was sonicated for 4 hours. A glassy carbon rotating disk electrode, which was dropcast with 6 μl of the ink mentioned above (1.91 mg $cm^{-2}$ of the catalyst), was used for the tests. The rotation speed of the disk was set to 900 rpm. The reference electrode used for these experiments was Ag/$AgNO_3$ in 0.1 M tetrabutylammonium perchlorate (TBAP) in MeCN solution.

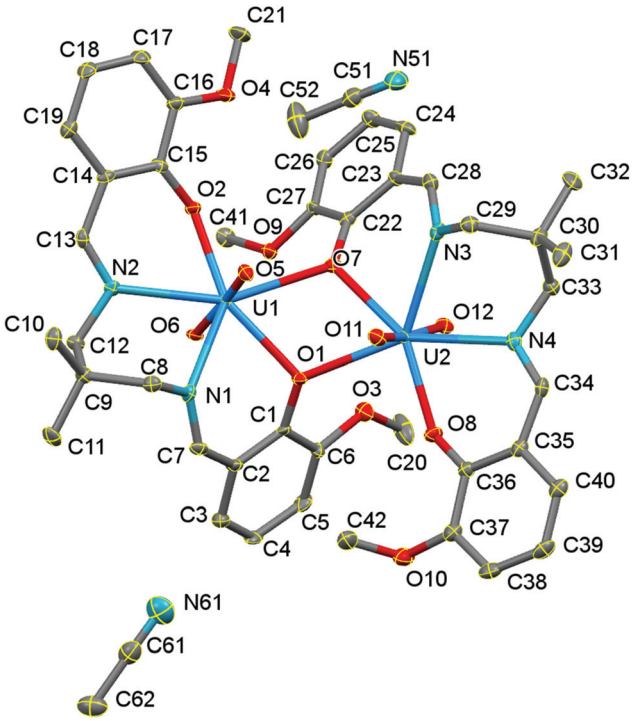


Fig. 1 The molecular structure of $[(UO_2)_2(L)_2]\cdot 2MeCN$, drawn with 50% probability of displacement ellipsoids of non-hydrogen atoms. The hydrogen atoms have been omitted for clarity.

## Results and discussion

### Description of the solid-state structure of the new uranyl complex from XRD

Single crystals of $[(UO_2)_2(L)_2]\cdot 2MeCN$ [Fig. 1] were obtained from the solutions of uranyl complex crystallized in MeCN, and the structure was solved and refined in the triclinic space group $P\bar{1}$. Details of the structure refinement and solution are given in the ESI Table S1.† The compound contains two deprotonated O^N^N^O 6,6′-((1*E*,1′*E*)-((2,2-dimethylpropane-1,3-diyl) bis(azaneylylidene))-bis-(methaneylylidene))bis(2-methoxyphenol) ligands and two $UO_2^{2+}$ units alongside with two co-crystallized MeCN molecules. Uranyl complexes with this type of bis(salicylidene)propanediamine ligand were previously reported with mononuclear or polynuclear coordination entities.[37–45] Each salen ligand binds to one uranyl *via* two imine N atoms, one terminal alkoxide and one bridging alkoxide ligand making up a seven-coordinated U(IV) atom in a pentagonal bipyramidal geometry.[46] The salicylidene-1-methaneaminato moieties are distorted from planarity (the endocyclic CC–C=N dihedral angles lie in range 15.7(2)–32.8°) as a result of the large size of $U^{6+}$ cation and the consequent increase of the distance between the coordinating atoms. For smaller cations and similar pure ligands, the salicylidene-1-methaneaminato

moieties are almost planar.[47–49] The mutual arrangement of the salicylidene-1-methaneaminato moieties in both ligand molecules is different, and the dihedral angle between all non-hydrogen atoms of these moieties are 27.7(2) and 32.3(2)°. The analysis of C–N bond lengths shows that the double bonds are fully localised within benzylideneamino moieties (ESI Table S2†).

The weak C–H···O intramolecular hydrogen bonds[48] (ESI Table S3†) provide some linkage between the complex and solvent MeCN molecules. The possibility of π···π stacking, which has been observed in related complexes,[50] is probably impeded in this structure by the large dihedral angle between planes of neighboring aromatic rings (larger than 32°).

The UV-vis absorption spectrum of the compound is characterized in the visible range by a broad absorption band centered at 425 nm ($\varepsilon$ = 1420 $M^{-1}$ $cm^{-1}$). This band can be assigned to a ligand (multidentate hydroxyl groups)-to-metal (uranyl ions) charge transfer in line with previous reports of similar complexes.[51,52] Bands of higher intensity were found at 330 nm and 300 nm, that can be assigned to LMCT within the uranyl cation.[51,52] The intense bands at 380 and 220 nm dominating the UV range were assigned to p–p* transitions within the organic ligand.[51,52] The observed absorption of the UV-vis light excites electrons from the valence band (VB) to the conduction band (CB), leaving "positive holes" in the VB. The photogenerated electrons and positive holes migrate to the surface of the photocatalyst during which some of the electrons and holes recombine and release energy in the form of emitted light of longer wavelength to harvest solar light radiation, thus confirming the photocatalytic potential of the compound [Fig. S1†].

### Photocatalytic reduction of $CO_2$

The photocatalytic reduction of $CO_2$ was performed in an MeCN–$H_2O$ system with TEOA as the sacrificial agent in a pre-conditioned reactor. The rate of methanol formation was observed to be 0.038 mmol $g^{-1}$ $h^{-1}$ in the MeCN–TEOA system. However, the rate of formation of methanol increased to 0.80 mmol $g^{-1}$ $h^{-1}$ with the addition of 0.5 mL water to the reaction. The addition of 1.0 mL and 2.0 mL water to the reaction system led to MeOH production rate of 1.08 and 1.29 mmol $g^{-1}$ $h^{-1}$, respectively. However, further increment in water concentration, *i.e.* 3.0 mL and 4.0 mL of water in the reaction system resulted in a marginal increase in the methanol formation at the rate of 1.31 and 1.35 mmol $g^{-1}$ $h^{-1}$, respectively [Fig. 2a]. Therefore, the optimum reaction medium for the photocatalytic reduction of $CO_2$ to $CH_3OH$ was selected to contain 16 mL MeCN, 2 mL $H_2O$ and 2 mL TEOA. Similarly, the effect of TEOA, keeping the amount of water constant, was monitored and 2 mL TEOA was found optimum to get the best possible rate of methanol production *i.e.* 1.29 mmol $g^{-1}$ $h^{-1}$ [Fig. 2b].

Taking into account the optimum reaction medium, the formation of $CH_4$ and oxygen was also observed [Table 1 and Fig. 3]. The formation of $O_2$ is possibly due to the oxidation of water by holes, and the presence of $O_2$ was also quantified using GC (the method included corrections for the presence of air in the sample and the use of Ar as the carrier gas). Specifically, 0.01 mmol $g^{-1}$ of $CH_4$, 30.84 mmol $g^{-1}$ of MeOH and 22.12 mmol $g^{-1}$ of $O_2$ were produced during the first 24 h [Table 1 and Fig. 3]. The rate of production of MeOH from the photocatalytic reduction of $CO_2$ was found to be 1.29 mmol $g^{-1}$ $h^{-1}$. Kumar and co-workers reported a MeOH yield of 3977.57 ± 5.60 μmol $g_{cat}^{-1}$ from the photocatalytic reduction of $CO_2$ after 48 h of illumination using a ruthenium trinuclear polyazine complex as a photocatalyst.[17] Li *et al.* reported a copper(II)imidazolate framework for the photocatalytic reduction of $CO_2$ to MeOH with a 1712.7 μmol $g^{-1}$ turnover in 5 h.[53] Comparison of the results shows that the title complex is an effective homogeneous catalyst for the photocatalytic reduction of $CO_2$.

The reaction progress was monitored up to 48 h, and the product formation rate remained consistent, yielding 0.03 mmol $g^{-1}$ of methane, 46.86 mmol $g^{-1}$ of methanol and 29.53 mmol $g^{-1}$ of $O_2$ (Table 1). The amount of $O_2$ being lower than the stoichiometric amount may originate from competition between TEOA and $H_2O$ as electron donors and the solubility of $O_2$ in the reaction mixture. After 48 h, the reaction

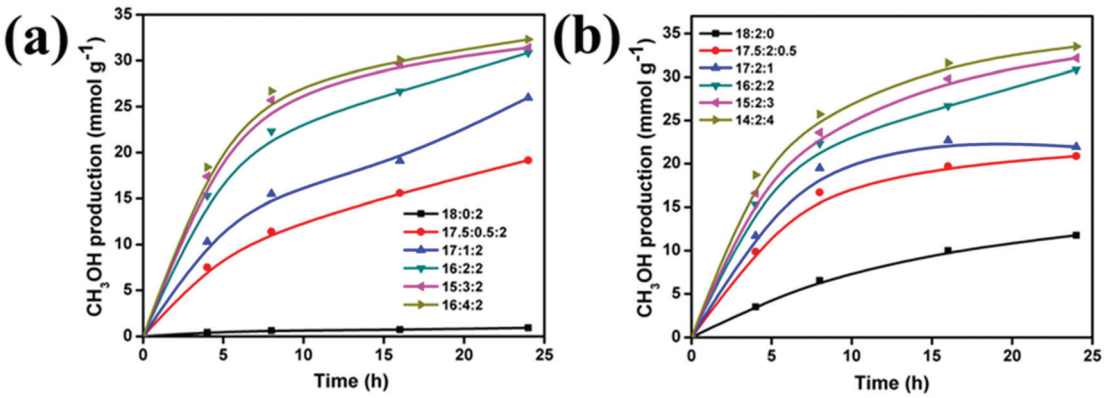


Fig. 2 Effect of the TEOA : $H_2O$ : MeCN ratio on the MeOH production. (a) Variation of $H_2O$ and (b) variation of TEOA. $CO_2$ pressure 1.1 bar, reaction mixture volume 20 mL with 5.0 mg catalyst under visible light irradiation.

 

Table 1 Photocatalytic reduction of $CO_2$ to $CH_4$, MeOH, and formation of $O_2$ (from $H_2O$) by the catalyst under visible light

| | $CH_4$ yield (mmol $g^{-1}$) | | MeOH (mmol $g^{-1}$) | | $O_2$ (mmol $g^{-1}$) | |
|---|---|---|---|---|---|---|
| Time (h) | MeCN + $H_2O$ | MeCN + $H_2O$ + TEOA | MeCN + $H_2O$ | MeCN + $H_2O$ + TEOA | MeCN + $H_2O$ | MeCN + $H_2O$ + TEOA |
| 24 | 0.025 | 0.01 | 11.76 | 30.84 | 12.93 | 22.12 |
| 48 | 0.043 | 0.03 | 13.59 | 46.86 | 16.85 | 29.53 |
| After 48 h, the reaction samples were purged with $CO_2$ | | | | | | |
| 72 | 0.031 | 0.02 | 23.81 | 74.33[a] | 14.29 | 27.84 |

[a] 500 μL of TEOA was further added to the reaction mixture.

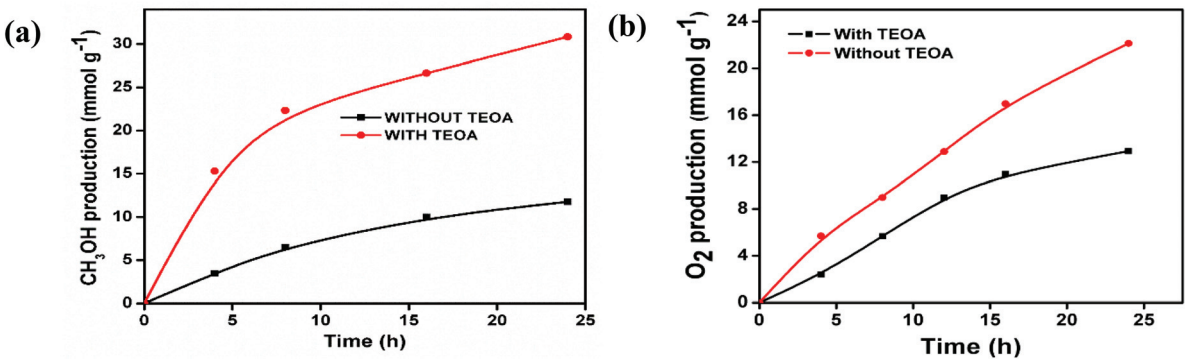


Fig. 3 Time-dependent effect of the MeCN : $H_2O$ : catalyst : visible light. (a) Selective formation of MeOH and (b) formation of $O_2$. Reaction conditions: $CO_2$ pressure 1.1 bar, reaction mixture volume 20 mL with 5.0 mg catalyst under visible light irradiation.

mixture was again purged with $CO_2$, and the reaction continued for the next 24 h (72 h of total reaction time). Further increases in MeOH production to 23.81 mmol $g^{-1}$ in the case of the MeCN + $H_2O$ mixture and 74.33 mmol $g^{-1}$ in the case of the MeCN + $H_2O$ + TEOA mixture (initially containing 500 μL of TEOA) were observed. On this basis, it can be concluded that the catalyst is stable, *i.e.*, there is no activity loss during the 48 h reaction time. The turnover number (TON) was calculated to be 39.36 after 24 h, while the turnover frequency (TOF) was found to be 1.64 $h^{-1}$. The light intensity reaching the interior of the reactor was 3.6 mW $cm^{-2}$ of visible light at 450 nm. Consequently, the calculated quantum yield (QY) of the catalyst under visible light was 18%. The TON and quantum yield obtained in the present study are also comparable to the recently reported homogeneous complex system for the photocatalytic reduction of $CO_2$ to fuels.[54–59] Next, the formation of hydrogen during the photocatalytic reduction of $CO_2$ was examined, and 242.82 and 282.60 μmol $g^{-1}$ of $H_2$ were produced in 24 h and 48 h, respectively [Fig. S2†]. The formation of $H_2$ in the presence of $CO_2$ could arise from the splitting of formic acid that was produced during the photocatalytic reduction of $CO_2$ with $H_2O$, as well as from the decomposition of water to $H_2$ and $O_2$ (determined in the gaseous products of the reaction). The formation of formic acid is confirmed using electrospray ionization-mass spectroscopy (ESI–MS) (discussed later in this manuscript).

To explain why the methanol production almost reached equilibrium at 24 h, a series of experiments with different amounts of methanol (10, 100 and 1000 μL) added into the MeCN + $H_2O$ + TEOA mixture were performed for 24 h. During these experiments, $CH_4$ was produced [Fig. S3†], and its formation rate increased with an increase in the initial amount of MeOH. This result indicates that higher concentrations of MeOH result in the production of more $CH_4$.

In addition, $^{13}C$ labeling was used to study the reaction. The MeCN + $H_2O$ mixture containing 0.5 mg of the catalyst and saturated with $^{13}CO_2$ was studied under visible light irradiation. After the photocatalytic reaction, the product was analyzed by $^1H$ and $^{13}C$ NMR. The signal at approximately 3.7 ppm [Fig. S4†] is associated with the $^1H$ of methanol. The shift in $^1H$ of methanol is caused by the influence of the nuclear magnetic moment of the $^{13}C$ on the hydrogen nucleus.[59] The $^{13}C$ signal at approximately 49.5 ppm [Fig. S5†] arose due to the presence of $^{13}CH_3OH$. These results confirmed that methanol was produced directly from the photocatalytic reduction of $CO_2$, and it was not produced from the photodissociation of the carbon-containing catalyst or solvent.

UV-vis absorption spectra were recorded during the photocatalytic process. The initial spectrum containing the catalyst in a MeCN : $H_2O$ mixture of 18 : 2 (v/v) showed absorption maxima at 367, 270 and 255 nm (Fig. 4).

Next, the solution was saturated with $CO_2$, and the UV-vis spectrum of this system was recorded. This spectrum was considerably different from the spectrum of the initial solution; *i.e.*, new absorption maxima at 341 and 263 nm were observed, and the maxima at 225 nm had a shoulder, suggesting a clea-

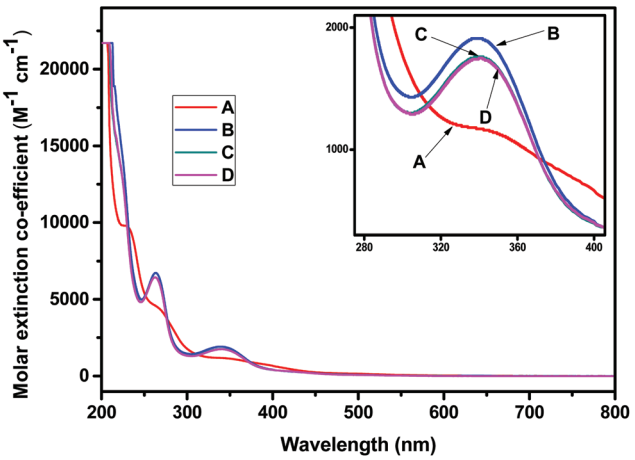


Fig. 4 UV-vis absorption spectra of the catalyst in the presence of $CO_2$. The spectra were recorded every 30 min after illumination with visible light. Inset: (A) Compound + MeCN + $H_2O$, (B) compound + MeCN + $H_2O$ + $CO_2$ + 30 min light irradiation, (C) compound + MeCN + $H_2O$ + $CO_2$ + 60 min light irradiation, (D) compound + MeCN + $H_2O$ + $CO_2$ + 90 min light irradiation.

vage in the bridging bond and formation of mononuclear complex units. After irradiation with visible light, the intensity of these newly formed absorption maxima decreased slowly, indicating the utilization of $CO_2$ in the reaction. The addition of $CO_2$ to the compound results in an eight- and a six-electron reduction of $CO_2$ to $CH_4$ and MeOH.

### Electrochemical activity

Cyclic voltammetry (CV) revealed that the presence of $CO_2$ in the electrolyte caused a significant increase in the current density *versus* the CV under $N_2$ bubbling [Fig. 5a], indicating a substantial electrochemical reduction activity in the presence of $CO_2$, which is a well-defined reduction process and associated with the reduction of $CO_2$.

The effect of the presence of water in the electrolyte was investigated by linear sweep voltammetry (LSV) tests under both $N_2$ and $CO_2$ bubbling. The studied compound is fairly active for the reduction of $CO_2$ in the absence of water in the electrolyte [Fig. 5b]. However, the higher amount of water increased the current densities, but the current densities recorded under $N_2$ bubbling exceeded those under $CO_2$ bubbling. This increase in the total current densities can be justified by an increase in the hydrogen evolution reaction (HER), which in the presence of water and at higher potentials tends to be dominant,[60] and consequently lowers the faradaic efficiency of the electrochemical reduction of $CO_2$.

To investigate the selectivity of the studied catalyst under $CO_2$ electrochemical reduction conditions, two electrodes were prepared (over titanium foil and carbon paper supports) with the same catalyst loading (1.91 mg $cm^{-2}$) but with a higher electroactive area (1 $cm^2$) to allow the quantification of products. In chronoamperometric tests under different applied potentials, the current densities ≤1 mA $cm^2$ were measured; the only detected liquid product was methanol, and the gaseous product was mainly $H_2$. The highest faradaic efficiency (*i.e.*, selectivity for $CO_2$ reduction) was achieved at −1.5 V *vs.* $Ag/AgNO_3$ in both electrode supports [Fig. S6†], although titanium foil was more suitable than carbon paper as the support for dropcasting this catalyst material. Hence, the highest production rate achieved after 3 h of testing was 5 μmol $cm^{-2}$ $h^{-1}$ (over Ti foil at −1.5 V *vs.* $Ag/AgNO_3$). The lower performance observed with the carbon paper support than with the Ti foil support can be explained first by the detachment of some electrocatalyst, and second by the fragility of the electrode itself when used in an H-type cell (like the one used in this work); *i.e.*, constant bubbling of $CO_2$ and magnetic stirring create a turbulent flow which causes the breaking of the support in some parts. Therefore, for future applications of this catalyst for the electrocatalytic reduction of $CO_2$, the deposition on the electrode surface must be optimized.

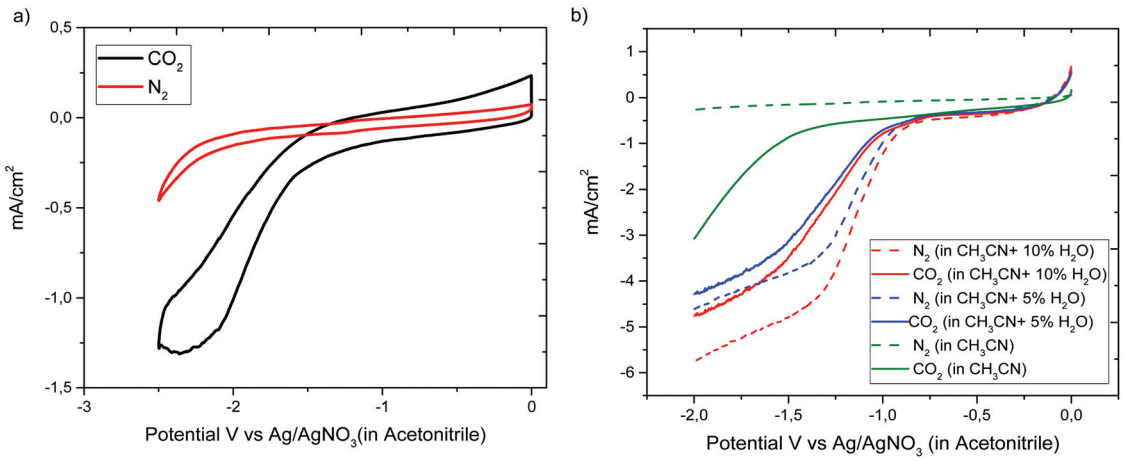


Fig. 5 (a) Cyclic voltammograms of the uranyl complex in 0.1 M $Bu_4NPF_6$/MeCN solution under argon (red trace) or $CO_2$ atmosphere (black trace). (b) Linear sweep voltammograms of the uranyl complex in 0.1 M $Bu_4NPF_6$/MeCN solution with different amounts of $H_2O$ in the electrolyte. Dashed lines represent $N_2$ bubbling, solid lines $CO_2$ bubbling through the solutions.

To trace complex species in the reaction solutions during catalytic $CO_2$ reduction and to describe a possible reaction mechanism, ESI–MS(+) experiments were conducted, and the results were summarized in Scheme 1. The ion with $m/z$ 1277.4394 matches exactly with the mass of the title complex when it exists as the +1 molecular ion. Furthermore, the presence of ions with $m/z$ = 639.226 in the ESI–MS spectra of the MeCN solution suggests that the compound can dissociate into a mononuclear uranyl species in solution [Fig. S7†]. The presence of ions with $m/z$ equal to 1277.43 and 639.22 in the reaction mixture before and after the 24 h photocatalytic reduction of $CO_2$ in MeCN + $H_2O$ + TEOA confirms that the identity of the catalyst remained intact even after the reaction, and the catalyst remained stable during the photocatalytic reduction of $CO_2$ [Fig. S8 and S9†]. The carbonate species formed from $CO_2$ dissolved in water was responsible for the production of formic acid, which, upon further reduction, was converted to MeOH.

During the photocatalytic reduction of $CO_2$, the interactions of solvent, reactants, intermediates and products with the compound are possible. The less populated ions observed in ESI–mass spectra represent the adducts with solvent, reactants, intermediates and products. Based on the ESI–mass spectra analysis, Scheme 1 has been developed. The ion with $m/z$ = 680.24 originates from the interaction of MeCN with species **2** and formation of species **3**. Further, species **3** upon

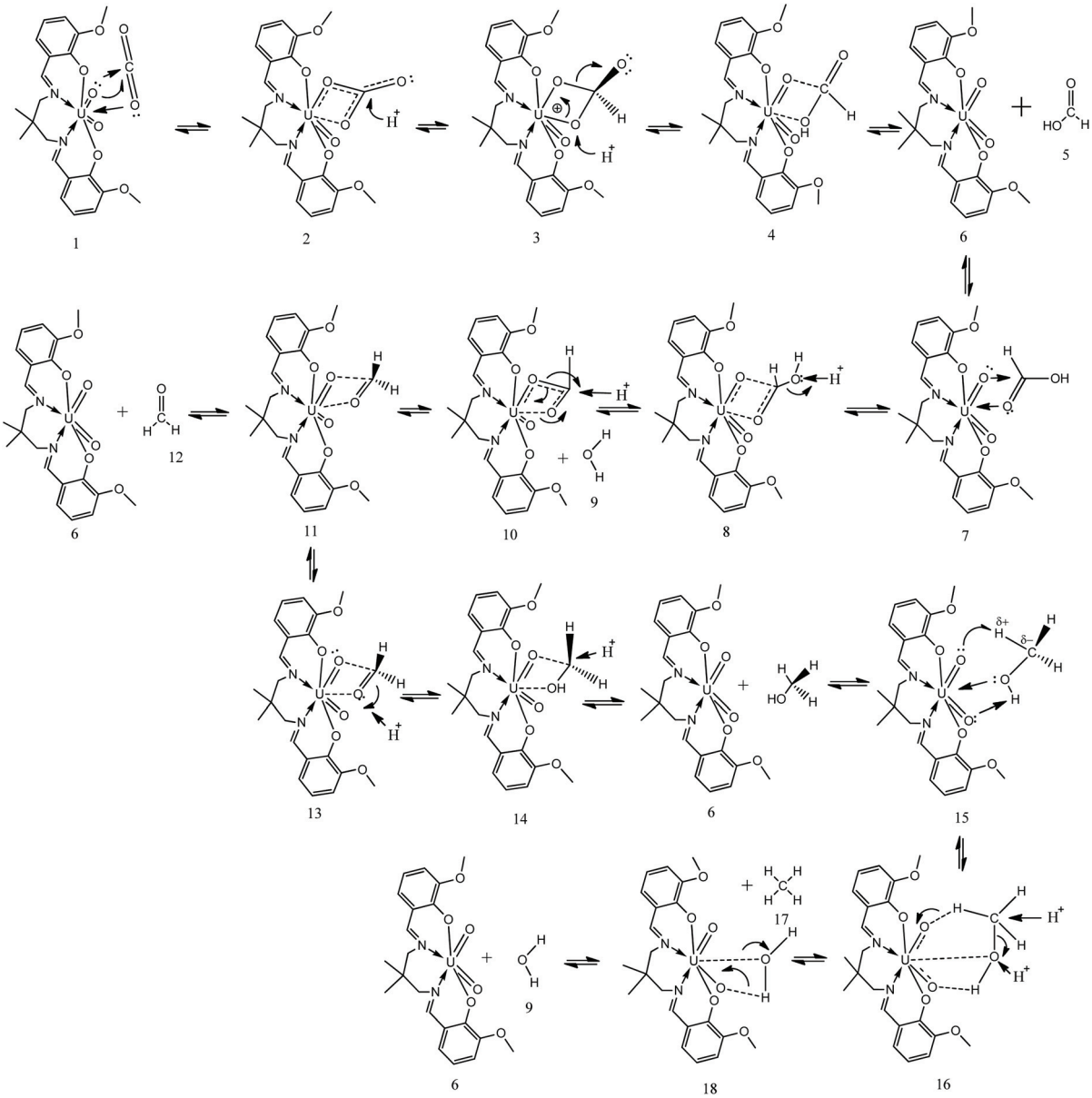


**Scheme 1** Proposed species from ESI–MS(+) experiments and proposed mechanistic pathway for the $CO_2$ reduction to MeOH with a mononuclear $[UO_2(L)]$ catalyst.

interaction with $H_2O$ can form **4** ($m/z$ = 657.23), which subsequently interacting with $CO_2$ undergoes photocatalytic reduction and forms formic acid. An observed ion with $m/z$ = 685.23 matches perfectly with the formic acid-attached **5**. Later, **5** undergoes a photocatalytic reduction of formic acid to methanol yielding **6** ($m/z$ = 671.25). Upon dissociation of methanol, **6** goes back to **2** or undergoes a further reduction of methanol to methane (**7**, $m/z$ = 655.25) followed by dissociation of methane and making **2** available to carry forward the next photocatalytic reduction of $CO_2$. Finally, a complete cycle of photocatalytic reduction of $CO_2$ over **2** has been observed by ESI–mass analysis of reaction mixture after 24 h. Some other combinations of reactants, products and intermediate products were also established on the basis of ESI–mass spectra analysis of the reaction mixture. The ion with $m/z$ = 741.3 may represent simultaneous interaction with the combination of MeCN, MeOH and CHO [ESI Scheme S1,† species **8**]. The ion with $m/z$ = 791.2 may originate from the interaction of **2** carbonate species and one of the products (ESI Scheme S1,† species **9**). The possible mechanistic route of the reduction of $CO_2$ to various products is shown in Scheme 1.

## Conclusion

A new binuclear uranyl complex containing a dianionic O^N^N^O tetradentate bis(salicylidene)propanediamine ligand was successfully synthesized and structurally characterized. When dissolved in solutions containing $H_2O$ and MeCN, the compound photocatalytically reduced $CO_2$ to MeOH under visible light irradiation with the MeOH formation rate of 0.49 mmol $g^{-1}$ $h^{-1}$. However, TEOA as the sacrificial donor has a positive effect on the photocatalytic reduction of $CO_2$ and doubles the MeOH formation rate. Compared with other systems, the MeOH production rate of 1.29 mmol $g^{-1}$ $h^{-1}$ is excellent at optimum reaction conditions. The catalyst was highly stable under the reaction conditions for at least 72 h as shown from ESI–MS measurements on the catalysis solutions. Both the binuclear complex and mononuclear species were observed. The nuclearity of the "real" catalyst is thus not unequivocal, but mononuclear species were assumed to be active. Experiments using labelled $^{13}CO_2$ showed that $CO_2$ is the exclusive source for the produced MeOH. Electrochemical experiments showed marked cathodic catalytic waves in the presence of $CO_2$. Although the main product from the photocatalysis was MeOH in all cases, sizable amounts of $CH_4$, $H_2$ and $O_2$ were also found from GC–MS analyses. A catalytic cycle for a mononuclear catalytic species was proposed based on a combination of *in situ* UV-vis, NMR and ESI–MS(+) experiments.

## Conflicts of interest

There are no conflicts to declare.

## Acknowledgements

The authors acknowledge funding from the Research and Development (R&D) Program (Research Pooling Initiative), Ministry of Education, Riyadh, Saudi Arabia, (RPI-KSU).

## References

1 H. Takeda, H. Kamiyama, K. Okamoto, M. Irimajiri, T. Mizutani, K. Koike, A. Sekine and O. Ishitani, *J. Am. Chem. Soc.*, 2018, **140**, 17241–17254.
2 T. Gasser, C. Guivarch, K. Tachiiri, C. Jones and P. Ciais, *Nat. Commun.*, 2015, **6**, 1–7.
3 S. Protti, A. Albini and N. Serpone, *Phys. Chem. Chem. Phys.*, 2014, **16**, 19790–19827.
4 G. Centi and S. Perathoner, *ChemSusChem*, 2010, **3**, 195–208.
5 W. Tu, Y. Zhou and Z. Zou, *Adv. Mater.*, 2014, **26**, 4607–4626.
6 S. C. Roy, O. K. Varghese, M. Paulose and C. A. Grimes, *ACS Nano*, 2010, **4**, 1259–1278.
7 S. N. Habisreutinger, L. Schmidt-Mende and J. K. Stolarczyk, *Angew. Chem., Int. Ed.*, 2013, **52**, 7372–7408.
8 J. O. Olowoyo, N. C. Hernández, M. Kumar, S. L. Jain, J. O. Babalola and U. Kumar, *ChemistrySelect*, 2018, **3**, 3659–3663.
9 J. O. Olowoyo, M. Kumar, N. Singhal, S. L. Jain, J. O. Babalola, A. V. Vorontsov and U. Kumar, *Catal. Sci. Technol.*, 2018, **8**, 3686–3694.
10 H. Tsubaki, A. Sekine, Y. Ohashi, K. Koike, H. Takeda and O. Ishitani, *J. Am. Chem. Soc.*, 2005, **127**, 15544–15555.
11 C. Bruckmeier, M. W. Lehenmeier, R. Reithmeier, B. Rieger, J. Herranz and C. Kavakli, *Dalton Trans.*, 2012, **41**, 5026–5037.
12 D. Behar, T. Dhanasekaran, P. Neta, C. Hosten, D. Ejeh, P. Hambright and E. Fujita, *J. Phys. Chem. A*, 1998, **102**, 2870–2877.
13 S. Sato, T. Morikawa, T. Kajino and O. Ishitani, *Angew. Chem., Int. Ed.*, 2013, **52**, 988–992.
14 J. Bonin, M. Chaussemier, M. Robert and M. Routier, *ChemCatChem*, 2014, **6**, 3200–3207.
15 S. Fernández, F. Franco, C. Casadevall, V. Martin-Diaconescu, J. M. Luis and J. Lloret-Fillol, *J. Am. Chem. Soc.*, 2019, **142**, 120–133.
16 Y. Liu, J.-H. Guo, X.-Y. Dao, X.-D. Zhang, Y. Zhao and W.-Y. Sun, *Chem. Commun.*, 2020, **56**, 4110–4113.
17 P. Kumar, B. Sain and S. L. Jain, *J. Mater. Chem. A*, 2014, **2**, 11246–11253.
18 D. J. Boston, C. Xu, D. W. Armstrong and F. M. MacDonnell, *J. Am. Chem. Soc.*, 2013, **135**, 16252–16255.
19 F. Bertini, M. Glatz, B. Stöger, M. Peruzzini, L. F. Veiros, K. Kirchner and L. Gonsalvi, *ACS Catal.*, 2018, **9**, 632–639.
20 A. R. Fox, S. C. Bart, K. Meyer and C. C. Cummins, *Nature*, 2008, **455**, 341–349.

21 M. Sundararajan, A. J. Campbell and I. H. Hillier, *J. Phys. Chem. A*, 2008, **112**, 4451–4457.
22 S. Kannan, A. E. Vaughn, E. M. Weis, C. L. Barnes and P. B. Duval, *J. Am. Chem. Soc.*, 2006, **128**, 14024–14025.
23 J. D. Wall and L. R. Krumholz, *Annu. Rev. Microbiol.*, 2006, **60**, 149–166.
24 S. Tsushima, *Inorg. Chem.*, 2009, **48**, 4856–4862.
25 P. L. Arnold, D. Patel, C. Wilson and J. B. Love, *Nature*, 2008, **451**, 315–317.
26 S. J. Formosinho, H. D. Burrows, M. da Graça Miguel, M. E. D. Azenha, I. M. Saraiva, A. C. D. Ribeiro, I. V. Khudyakov, R. G. Gasanov, M. Bolte and M. Sarakha, *Photochem. Photobiol. Sci.*, 2003, **2**, 569–575.
27 K. Vidya, V. Kamble, P. Selvam and N. Gupta, *Appl. Catal., B*, 2004, **54**, 145–154.
28 S. Kannan, M. A. Moody, C. L. Barnes and P. B. Duval, *Inorg. Chem.*, 2006, **45**, 9206–9212.
29 Y. Li, S. A. e. A. Rizvi, D. Hu, D. Sun, A. Gao, Y. Zhou, J. Li and X. Jiang, *Angew. Chem.*, 2019, **131**, 13633–13640.
30 P. L. Arnold, J. M. Purkis, R. Rutkauskaite, D. Kovacs, J. B. Love and J. Austin, *ChemCatChem*, 2019, **11**, 3786–3790.
31 Y. Li, G. Zhang, W. Eugen Schwarz and J. Li, *Inorg. Chem.*, 2020, **59**, 6287–6300.
32 S. Rayati, E. Khodaei, M. Jafarian, A. Bahrami, A. Wojtczak and A. Kozakiewicz, *J. Coord. Chem.*, 2017, **70**, 1424–1437.
33 G. M. Sheldrick, *Acta Crystallogr. Sect A: Found. Adv.*, 2015, **71**, 3–8.
34 G. M. Sheldrick, *Acta Crystallogr., Sect. C: Struct. Chem.*, 2015, **71**, 3–8.
35 G. M. Sheldrick, *Acta Crystallogr., Sect. A: Found. Crystallogr.*, 2008, **64**, 112–122.
36 E. Prince and A. J. C. Wilson, *Int. Tables Crystallogr*, Kluwer, 2004.
37 D. Mentzafos, A. Hountas, H. Tajmir-Riahi and A. Terzis, *Acta Crystallogr., Sect. C: Cryst. Struct. Commun.*, 1987, **43**, 1500–1502.
38 M. Azam, S. I. Al-Resayes, G. Velmurugan, P. Venuvanalingam, J. Wagler and E. Kroke, *Dalton Trans.*, 2015, **44**, 568–577.
39 M. Azam, G. Velmurugan, S. M. Wabaidur, A. Trzesowska-Kruszynska, R. Kruszynski, S. I. Al-Resayes, Z. A. Al-Othman and P. Venuvanalingam, *Sci. Rep.*, 2016, **6**, 32898.
40 M. Azam, S. I. Al-Resayes, M. Alam, N. T. M. Albaqami, S. Park, A. Trzesowska-Kruszynska and R. Kruszynski, *J. Mol. Struct.*, 2017, **1150**, 395–403.
41 L. Salmon, P. Thuéry and M. Ephritikhine, *Acta Crystallogr., Sect. C: Cryst. Struct. Commun.*, 2003, **59**, m246–m248.
42 D. J. Evans, P. C. Junk and M. K. Smith, *Polyhedron*, 2002, **21**, 2421–2431.
43 L. Salmon, P. Thuéry and M. Ephritikhine, *Dalton Trans.*, 2004, 1635–1643.
44 L. Salmon, P. Thuéry and M. Ephritikhine, *Dalton Trans.*, 2004, 4139–4145.
45 L. Salmon, P. Thuéry and M. Ephritikhine, *Polyhedron*, 2006, **25**, 1537–1542.
46 D. Kepert, *Prog. Inorg. Chem.*, 1979, **25**, 41–144.
47 J. Corden, W. Errington, P. Moore and M. Wallbridge, *Acta Crystallogr., Sect. C: Cryst. Struct. Commun.*, 1996, **52**, 125–127.
48 G. R. Desiraju and T. Steiner, The weak hydrogen bond: in structural chemistry and biology, *Int. Union Crystallogr. Monogr. Crystallogr.*, 2001, **9**, 1–409.
49 A. Thevenon, J. A. Garden, A. J. White and C. K. Williams, *Inorg. Chem.*, 2015, **54**, 11906–11915.
50 R. Kruszynski and T. Sierański, *Cryst. Growth Des.*, 2016, **16**, 587–595.
51 M. S. Bharara, K. Heflin, S. Tonks, K. L. Strawbridge and A. E. Gorden, *Dalton Trans.*, 2008, 2966–2973.
52 M. S. Bharara, K. Strawbridge, J. Z. Vilsek, T. H. Bray and A. E. Gorden, *Inorg. Chem.*, 2007, **46**, 8309–8315.
53 J. Li, D. Luo, C. Yang, S. He, S. Chen, J. Lin, L. Zhu and X. Li, *J. Solid State Chem.*, 2013, **203**, 154–159.
54 A. M. Cancelliere, F. Puntoriero, S. Serroni, S. Campagna, Y. Tamaki, D. Saito and O. Ishitani, *Chem. Sci.*, 2020, **11**, 1556–1563.
55 D. Hong, T. Kawanishi, Y. Tsukakoshi, H. Kotani, T. Ishizuka and T. Kojima, *J. Am. Chem. Soc.*, 2019, **141**, 20309–20317.
56 K. Kamada, J. Jung, W. Taku, K. Sekizawa, S. Sato, T. Morikawa, S. Fukuzumi and S. Saito, *J. Am. Chem. Soc.*, 2020, **142**, 10261–10266.
57 Y. Qin, L. Chen, G. Chen, Z. Guo, L. Wang, H. Fan, M. Robert and T.-C. Lau, *Chem. Commun.*, 2020, **56**, 6249–6252.
58 A. Umemoto, Y. Yamazaki, D. Saito, Y. Tamaki and O. Ishitani, *Bull. Chem. Soc. Jpn.*, 2020, **93**, 127–137.
59 Y. Jia, Y. Xu, R. Nie, F. Chen, Z. Zhu, J. Wang and H. Jing, *J. Mater. Chem. A*, 2017, **5**, 5495–5501.
60 J. Zeng, T. Rino, K. Bejtka, M. Castellino, A. Sacco, M. A. Farkhondehfal, A. Chiodoni and F. Drago, *ChemSusChem*, 2020, **13**, 4128–4139.